Optical Properties Influence Visual Cortical Functional Resolution After Cataract Surgery and Both Dissociate From Subjectively Perceived Quality of Vision

Ângela Sofia Cardoso Miranda,[1,2] Andreia de Faria Martins Rosa,[3] Miguel José Patrício Dias,[3,4] Ben M. Harvey,[5] Maria Fátima Loureiro da Silva,[1] Miguel de Sá e Sousa Castelo-Branco,[1–3,6] and Joaquim Carlos Neto Murta[3,7]

[1]Institute for Biomedical Imaging in Life Sciences (IBILI), Faculty of Medicine of the University of Coimbra, Coimbra, Portugal
[2]Institute of Nuclear Sciences Applied to Health (ICNAS), University of Coimbra, Coimbra, Portugal
[3]Faculty of Medicine of the University of Coimbra, Coimbra, Portugal
[4]Laboratory of Biostatistics and Medical Informatics and IBILI, Faculty of Medicine of the University of Coimbra, Coimbra, Portugal
[5]Experimental Psychology, Helmholtz Institute, Utrecht University, Utrecht, The Netherlands
[6]Brain Imaging Network of Portugal, Coimbra, Portugal
[7]Ophthalmology Department, Centro Hospitalar e Universitário de Coimbra, Coimbra, Portugal

Correspondence: Miguel Castelo-Branco, ICNAS Polo 3, 3000-548 Coimbra, Portugal; mcbranco@fmed.uc.pt.

ASCM and AdFMR contributed equally to the work presented here and should therefore be regarded as equivalent first authors.

MSCB and JCNM contributed equally to the work presented here and should therefore be regarded as equivalent senior authors.

Submitted: May 31, 2017
Accepted: December 29, 2017

Citation: Miranda ÂSC, Martins Rosa AF, Patrício Dias MJ, et al. Optical properties influence visual cortical functional resolution after cataract surgery and both dissociate from subjectively perceived quality of vision. *Invest Ophthalmol Vis Sci*. 2018;59:986–994. https://doi.org/10.1167/iovs.17-22321

Purpose. To investigate the relation between optical properties, population receptive fields (pRFs), visual function, and subjectively perceived quality of vision after cataract surgery.

Methods. The study includes 30 patients who had recently undergone bilateral sequential cataract surgery. We used functional magnetic resonance imaging and pRF modelling methods to assess pRF sizes across visual cortical regions (V1–V3). Subjects also performed a complete ophthalmologic and psychophysical examination and answered a quality of vision questionnaire.

Results. Subjects with worse optical properties had, as predicted, larger pRF sizes. In addition, analysis in the primary visual cortex revealed significantly larger mean pRF sizes for operated subjects with worse contrast sensitivity ($P = 0.038$). In contrast, patients who scored high in the subjective "bothersome" dimension induced by dysphotic symptoms had surprisingly lower pRF size fitting interception ($P = 0.012$) and pRF size fitting slopes ($P = 0.020$), suggesting a dissociation between objective quality of vision and subjective appraisal.

Conclusions. Optical properties of the eye influence pRF size. In particular, visual aberrations have a negative impact on visual cortical processing. A novel dissociation between subjective reports of quality of vision and pRF sizes was further identified. This suggests that patients with better cortical resolution may have a negative subjective response possibly because of improved perception of dysphotic phenomena. pRF properties represent a valuable quantitative measure to objectively evaluate quality of vision but do not necessarily predict subjective complaints.

Keywords: quality of vision, fMRI, population receptive fields, dysphotic symptoms, visual cortical processing

Topographic mapping of the human visual cortex (cortical retinotopy) using noninvasive neuroimaging techniques plays a relevant role in understanding visual function and can be achieved by using functional magnetic resonance imaging (fMRI).[1–3] Multiple efforts have been made to identify and efficiently characterize properties of the human visual field maps. Engel et al.[4] have introduced a phase-encoding method to characterize the activity of the human visual cortex in both health and disease, taking advantage of the retinotopic organization of the visual system.[5–9]

More recently, a population receptive field (pRF) modelling approach has been proposed by Dumoulin and Wandell.[10] By incorporating an explicit model of neural response preferences, pRF modelling provides information about the receptive field (resolution) properties underlying fMRI responses. A pRF can be seen as the aggregate receptive field of the many neurons within an fMRI voxel that respond to stimulation of a particular retinal location.[11,12] Smaller pRFs reflect more fine-tuned visual processing, effectively increasing the spatial resolution of the visual system, while large pRFs reflect a coarser neural representation of visual space.[13,14] pRF sizes are influenced by eccentricity, with the smallest pRFs (reflecting underlying single-neuron receptive fields) being present in the neural representation of the central visual field, where visual acuity is greatest.[10,15,16] pRFs also vary hierarchically between visual areas, having smaller sizes in the primary visual cortex (V1).

pRF properties have been used to evaluate adaptive changes in the human brain resulting from diseases, trauma, and degeneration, with pRF changes mirroring changes in visual function.[13,17–22] pRF properties might also be used to help us understand how the optical properties of the eye influence the functional response properties of the visual cortex.

Recent studies suggest an association between perceptual acuity and neuronal population tuning in the primary and secondary visual cortex[13] and between acuity thresholds and cortical magnification in V1.[23] However, although optical parameters of the eye influence the processing of visual information, their impact on pRF sizes remains unclear. Moreover, the relation of these parameters with subjectively perceived quality of vision in the context of refractive surgery remains to be clarified.

Optical properties are an important outcome measure as they can be objectively measured and are not influenced by patients' collaboration. Wavefront analysis with a ray-tracing aberrometer was performed because it has been proven to provide reliable measurements despite the presence of a multifocal intraocular lens. Wavefront analysis provides a detailed assessment of the optical quality of each system (eye), including information on overall light deviation from the ideal focus plane (total root-mean-square), loss of image contrast (modulation transfer function), and point light distortion (Strehl ratio). More importantly, wavefront analysis is able to differentiate those refractive errors that are correctable with spectacles (lower-order aberrations) from those that are not (higher-order). This information, therefore, goes beyond classical outcomes (sphere, cylinder, and visual acuity). The optical properties evaluated in this study provide objective information on quality of vision, which can serve as a ground truth to validate the pRF method.

This study aims to evaluate the association between pRF size, visual function (including visual acuity), subjectively perceived quality of vision, and optical properties of the eye, including wavefront analysis. This approach is relevant to understand how the human brain adapts on a short-term basis to the imperfections of each visual system (eye) and optical interventions.[24–27] Therefore, we opted to study patients with recent cataract surgery and, consequently, with a changed optical visual system, before the occurrence of long-term adaptive changes.[28] We expected that worse optical properties are accompanied by large pRF sizes and investigated their relation with subjective quality of vision. Afferent resolution, as determined by optical properties, must influence efferent resolution, since pRFs essentially measure cortical resolution. To study the influence of optical properties on pRF sizes, it is necessary to separate this influence from adaptive changes that occur over time. It is known that subjects adapt on a long-term basis to the blur of their own optical systems. Studying recently operated patients allows us to assess on a short-term basis the influence of optical properties on pRF sizes because we measure the impact of intervention at a well-defined time point

Materials and Methods

Subjects

This cross-sectional study included 30 patients younger than 75 years, who received bilaterally diffractive bifocal intraocular lenses. Inclusion criteria comprised the following: no surgical complications, preoperative sphere inferior to 6 diopters (D) in magnitude in either eye, regular topography with less than 1.5 D of astigmatism, no history of previous corneal or intraocular surgery, absence of other ocular comorbidities and of metallic foreign bodies. Nontoric multifocal lenses (Acrysof Restor SN6AD1 IOL with a +3.00 addition; Alcon Surgical, Fort Worth, TX, USA) were implanted binocularly, with approximately a 1-week interval.

Additionally, we included 15 age- and sex-matched controls as proof of concept. Controls were recruited from the general ophthalmology clinic, fulfilling the following criteria: distance corrected visual acuity $\geq$ 20/25 and normal ophthalmic examination.

The study adhered to the tenets of the Declaration of Helsinki and was approved by the Ethical Committee of the Faculty of Medicine of the University of Coimbra. All subjects were given an information letter, followed by the clarification of any questions that might have arisen. All participants were adequately informed and signed the informed consent form.

Ophthalmologic Examination

At the third week after the second eye surgery, a complete ophthalmologic examination was performed, comprising uncorrected and corrected distance and near visual acuities, distance-corrected near visual acuity, uncorrected and distance-corrected intermediate visual acuity, slit-lamp examination, tonometry, and fundoscopy.

Distance visual acuity was measured by using ETDRS charts and near visual acuity by using the Portuguese version of the Radner test (Rosa AM, et al. *IOVS* 2016;57:ARVO E-Abstract 3756). All measurements were performed under photopic conditions (80 cd/m^2).

Optical Properties

We used the iTrace (version 6.0.1; Tracey Technologies, Houston, TX, USA), which combines an aberrometer with corneal topography, to obtain total ocular and internal aberrations, Strehl ratio, and modulation transfer function. The best-quality scan of the three manual measurements at 4 mm (after pupil dilation) was selected for further analysis. We evaluated total root-mean-square (total RMS: overall light deviation from the ideal focus plane; larger values reflect worse optical properties) and RMS of higher-order aberrations (HOAs) from third- to fifth-order Zernike coefficients (RMS of HOAs: those refractive errors that are not correctable with spectacles or soft contact lenses; larger values also reflect worse optical properties). We also measured average modulation transfer function height (MTF_h: a measurement of image contrast; higher values reflect better image contrast), modulation transfer function at 10 cycles per degree (cyc/deg), and the Strehl ratio. Strehl ratio is the ratio of the peak intensity of a point light source formed by the optical system (eye) compared to the maximum attainable intensity (formed by a perfect optical system). Values closer to 1 reflect better optics. All these parameters were recorded for corneal, internal, and total ocular optics. Values were extracted without spherico-cylindrical correction. All wavefront data were obtained from right eyes. Left eye values were similar.

In controls these parameters were corrected to approach as close as possible the clinical reality and to enable the study of correlations between symptoms, optical properties, and functional outcomes. The same rationale was applied to psychophysical assessment and fMRI.

Quality of Vision Questionnaire

Using the Quality of Vision (QoV) questionnaire, subjects rated 10 visual symptoms (glare, haloes, starburst, hazy vision, blurred vision, distortion, double or multiple images, fluctuation, focusing difficulties, distance or depth perception difficulties) in three subscales (frequency, severity, and bothersome).[29] Raw questionnaire data were Rasch-scaled to provide interval-level measurement properties.[30]

Magnetic Resonance Imaging

Stimulus Presentation and Apparatus. We generated our visual field mapping stimulus in MATLAB (version R2014b;

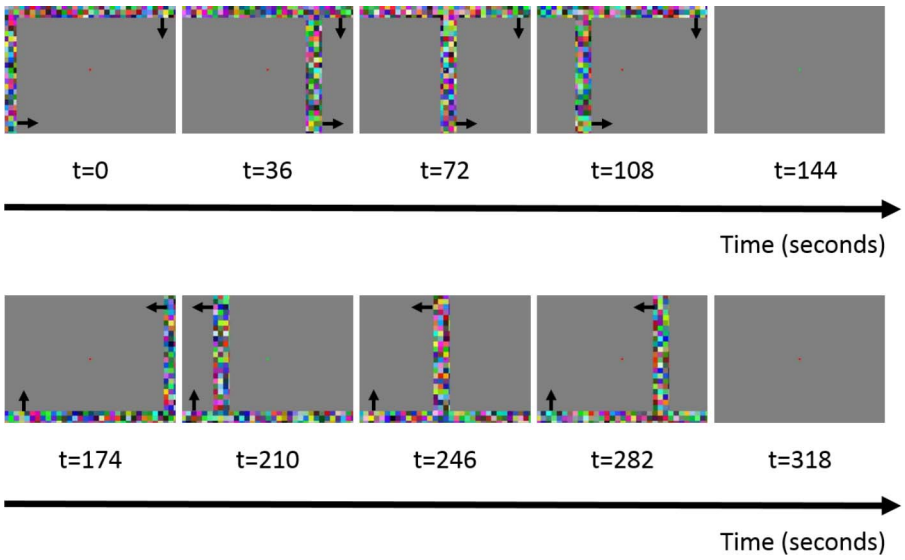

Figure 1. Illustration of simultaneous bars mapping stimuli. The *arrows* indicate the motion direction of the bars.

Mathworks, Natick, MA, USA), using the Psychophysics Toolbox.[31] The visual stimulus was displayed on a 32-inch NNL LCD monitor (InroomViewingDevice; NordicNeuroLab, Bergen, Norway) at a resolution of 1920 × 1080 pixels positioned at the end of the magnet bore of the scanner and viewed through a mirror attached to a head coil. The display was 70 × 39.5 cm and the viewing distance was 156.5 cm, so it subtended a 22.21° × 14.38° visual angle.

Simultaneous Bars Stimuli. We developed a new visual stimulus to increase mapping efficiency and fMRI response amplitudes. It consisted of two perpendicular bars that crossed the display in different phases and orthogonal directions. This design has previously increased mapping efficiency,[32] although here we used horizontal and vertical bars, subtending 1.80° and 1.57° of visual angle, respectively,[10,14,32,33] rather than wedges and rings.[10,14] Within these bar apertures, we displayed a colored checkerboard pattern, with the color of each square flickering between randomly chosen RGB color values on each frame.[34] The horizontal bars moved vertically across the display in 18 equally spaced steps, while the vertical bars moved horizontally across the display in 24 equally spaced steps. Each bar position was presented for 2 seconds to synchronize with the fMRI volume of acquisition.

The high-contrast horizontal and vertical bars each crossed the display repeatedly, with the horizontal bars taking 36 seconds to complete a full cycle and the vertical bars taking 48 seconds (Fig. 1). These asynchronous cycles allow pRF modelling to determine pRF positions in both dimensions simultaneously.[32] After 144 seconds, a 30-second period of mean luminance (zero-contrast) was displayed, providing a "blank" period that allows pRF models to determine the baseline fMRI response amplitude.[10,14,33]

In the first 144 seconds of each scanning run, the horizontal bars travelled downwards and the vertical bars travelled leftwards. After the blank period, both horizontal and vertical bars travelled in the opposite direction.

Participants were instructed to fixate a point in the center of the visual stimulus. The colors changed between red and green at random intervals, from 1.5 to 6 seconds. To ensure attention and fixation, participants pressed a button each time they detected a color change.

Data Acquisition. Magnetic resonance images (MRI) were acquired on a 3-Tesla Magneton TIM Trio scanner equipped with a 32-Channel Head Coil (Siemens, Erlangen, Germany).

Two high-resolution 3D anatomic MPRAGE (magnetization prepared rapid-acquisition gradient echo) images were acquired by using a standard T_1-weighted gradient eco (GE) pulse sequence (field of view [FOV] = 256 × 256 mm, 176 slices, voxel size = 1 × 1 × 1 mm, repetition time [TR] = 2.530 ms, echo time [TE] = 3.42 ms, inversion time [TI] = 1.100 ms, 7° flip angle).

Functional MRI images were recorded by using a T_2-weighted GE echo-planar imaging sequence over three runs at an isotropic resolution of 2 mm (FOV 256 × 256 mm), with 29 interleaved slices oriented orthogonally to the calcarine sulcus with no gap. TE was 30 ms, TR was 2000 ms, and flip angle was 90°. Each functional run was acquired by using 180 time frames (360 seconds).

Anatomic and Functional Preprocessing

All image data were processed and analyzed by using the BrainVoyager QX software (version 2.8.2; Brain Innovation B.V., Maastricht, The Netherlands).

Anatomic images underwent brain extraction and intensity normalization to reduce artifacts and inhomogeneity caused by the magnetic field.[35] The two anatomic data sets were then aligned to each other and averaged to improve the signal-to-noise ratio.[36] The resulting images were converted to the Talairach reference system.[37] Thereafter, white matter was segmented by using an automatic segmentation routine[38] and small manual adjustments were made. Mesh representations of each hemisphere were then created.[39,40]

The first six volumes of each experimental run were excluded from the analysis owing to early magnetization transients. Functional data preprocessing included slice scan time correction, linear trend removal, temporal high-pass filtering (2 cycles per run), and 3D interscan head motion correction with cubic spline interpolation. All functional volumes were corrected for motion within and between scan. As the head motion was minimal (≤2 mm in any direction), no block was excluded.

The preprocessed functional runs were coregistered with each subject's structural scan in Tailarach space and then averaged across scans.

Investigative Ophthalmology & Visual Science

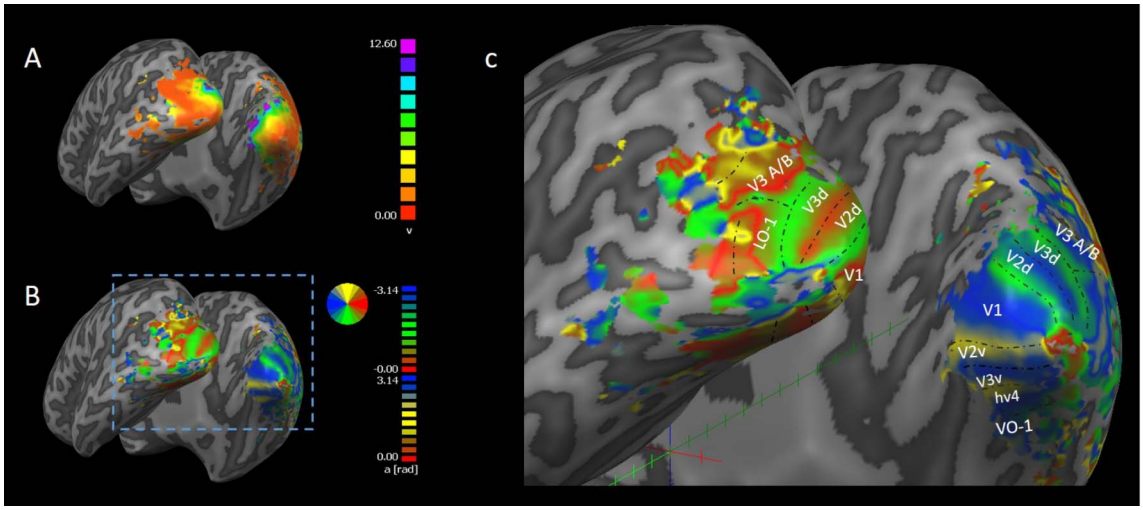

FIGURE 2. Visual field maps estimated for a subject. Eccentricity (**A**) and polar angle (**B**) maps, pooled from the pRF position parameters, were rendered on the inflated meshes and used to identify the boundaries of the visual areas (**C**). The colors represent the recording sites for which the pRF model explains at least 30% of the variance. *Black lines* and *labels* indicate the position of the visual areas identified in both hemispheres.

Population Receptive Field Modelling and Analysis

pRF models were estimated from BOLD responses to the simultaneous bars moving stimuli by using a model-driven approach developed by Dumoulin and Wandell[10] in 2008 and recently implemented in BrainVoyager QX (2013). Briefly, the pRF approach estimates a neural response model, for each voxel, that best explains the cortical visual field responses to a wide range of stimulus positions.[10,14]

First, we generated a binary stimuli frame containing detailed information about the sequence of visual field positions covered by the bars in the stimulus. Then, a large set of candidate pRF models was used to sample the frame and calculate at each time point (frame) a neural response strength that depends on the overlap between the stimulus and the Gaussian model.[41] These candidate neural response time courses were each convolved with a canonical hemodynamic response function to predict, for each set of candidate pRF parameters, the BOLD response time course that the stimulus would yield. The candidate response predictions were each compared against the measured response of every voxel. The pRF model that most closely fits the measured response of each voxel was chosen, giving the goodness of model fit (variance explained), the pRF size (σ), and preferred position (x and y). These position preferences were converted to preferred eccentricity and polar angle to delineate each visual field map.

The resulting parameter maps were projected on the inflated meshes. Retinotopic areas were manually drawn for each subject from the polar angle and eccentricity maps (Fig. 2).[11,42–44] Although we could identify visual field maps, we restricted our analysis to the primary visual cortex.

All the voxels with a poor pRF model fit, that is, with less than 30% of the variance explained, were removed from the analysis, as well as the voxels outside of the delineated region of interest. We also excluded voxels with pRF eccentricities below 0.5°, since this part of the visual field is difficult to accurately map, and those outside of the limits of the central vision (5° of eccentricity).[45] The retinotopy evaluated a wider field of vision because it is important to accurately map the different visual areas. Concerning pRF sizes, we limited its evaluation to the central 5° to be able to correlate and compare with optical properties, which were analyzed centered on the visual axis. Peripheral vision is prone to influences by other factors, such as the edge of the capsulotomy performed during cataract surgery. In addition, it is not always possible to correctly acquire larger optical zones, especially in older patients, who often have smaller pupils and incomplete pupil pharmacologic dilation.

Statistical Analysis

We developed a MATLAB script that allows to obtain pFR size and visual field maps for each participant. To study the relationship between pRF sizes and measured optical properties we extracted, for each participant, the mean pRF sizes to the central vision (0.5°–5° of eccentricity) and made comparisons using Mann-Whitney U tests. We also used regression analysis to study the relationship between pRF sizes and optical properties across eccentricity, by organizing the data into bins of 0.5° of eccentricity. Eccentricity-binned data were fitted by linear regression analysis as in the study by Harvey and Dumoulin,[14] obtained pRF size fitting interception (β_0) and pRF size fitting slope (β_1) for each participant. The beta regression parameters were also compared by using t-tests.

Finally, we investigated the relationship between the perceived quality of vision and the pRF measures, The questionnaire data were Rasch-scaled to provide separate subscales (frequency, severity, and bothersome),[46] and the intraocular lens (IOL) groups were divided into two subgroups on the basis of median value. The comparison between the subgroups was performed as described above.

RESULTS

The boundaries of area V1 were straightforwardly defined for all subjects. The resulting visual field maps in both groups showed a well-defined retinotopic organization of subjects with IOLs (Supplementary Fig. S1).

We compared the mean pRF sizes in the early visual cortex between groups and the changes of the pRF sizes across visual field eccentricities between groups. Figure 3 shows the regression line for the groups of patients and the control sample. There were no significant differences between the mean pRF and, as expected, the pRF sizes increased with eccentricity and across the visual field hierarchy (V1, V2, and V3).

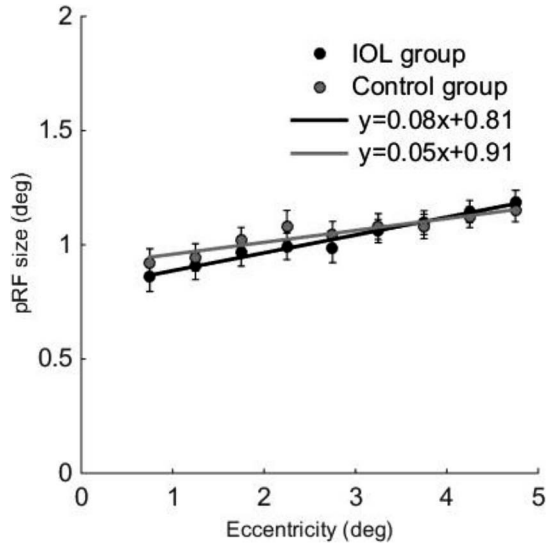

Figure 3. Changes in pRF size across visual field eccentricity in primary visual cortex. *Error bars* reflect the standard error of the mean (SEM) within each eccentricity bin. The *solid lines* represent the best-fitting functions (significant regressions, $P < 0.0001$) described by the equation$y = \beta_1 x + \beta_0$, where y is the pRF size, x is the eccentricity, and β_1 and β_0 are the slope and intercept, respectively. The 95% confidence intervals of these fits were determined by bootstrapping the binned data and refitting. No significant difference was found between groups: P value ($\beta 1$) = 0.103 and P value ($\beta 0$) = 0.133.

Optical Parameters and pRFs

To investigate the influence of optical parameters on cortical resolution, we divided the IOL group into subgroups according to median optical parameters (Tables 1, 2). Subjects' total RMS, RMS_h, modulation transfer function at 10 cyc/deg, and Strehl ratio values equal or above the median were assigned to the group labeled as "++", while the remaining were assigned to the group "–" (Table 2). Changes in pRF size as a function of visual field eccentricity in the primary visual cortex of these subgroups are shown in Figure 4 and Supplementary Figures S2 through S5. Our analysis revealed, as predicted, that subjects with worse optical resolution have larger pRF sizes, validating the use of the pRF technique. In particular, significant differences were found between the mean pRF size of the subgroups defined on the basis of MTF_h ($P = 0.038$, Mann-Whitney test).

Wavefront analysis results depend on the chosen optical zone and patients' age. The normative values for an age- and sex-matched group are displayed in Table 1 and were

Table 1. Optical Parameters Obtained for Patients Implanted With Multifocal IOLs at the Third Postoperative Week and for the Control Group as Acquired With Spectacle Correction

Optical Parameters	IOL Group, Mean (SD)	Control Group, Mean (SD)
RMS total	0.424 (0.129)	0.432 (0.127)
RMS_h	0.164 (0.051)	0.164 (0.052)
MTF_h	0.313 (0.065)	0.310 (0.065)
MTF at 10 cyc/deg	0.294 (0.101)	0.289 (0.100)
Strehl ratio	0.068 (0.034)	0.067 (0.035)

The values were accessed by using iTrace, which combines an aberrometer with corneal topography, for each eye, and the mean was calculated for each participant. SD, standard deviation; MTF, modulation transfer function.

Table 2. Optical Parameters Obtained for Subgroups Defined by Median Optical Parameter Value

	RMS Total		RMS_h		MTF_h		MTF at 10 cyc/deg		Strehl Ratio	
Optical Parameters	Group ++	Group –	Group ++	Group –	Group ++	Group –	Group ++	Group –	Group ++	Group –
RMS total	0.431 (0.130)	0.414 (0.124)	0.424 (0.132)	0.421 (0.122)	0.414 (0.124)	0.431 (0.130)	0.414 (0.124)	0.431 (0.130)	0.414 (0.124)	0.431 (0.130)
RMS_h	0.164 (0.053)	0.160 (0.048)	0.164 (0.051)	0.160 (0.049)	0.160 (0.048)	0.164 (0.053)	0.160 (0.048)	0.164 (0.053)	0.160 (0.048)	0.164 (0.053)
MTF_h	0.310 (0.067)	0.316 (0.066)	0.313 (0.065)	0.314 (0.066)	0.316 (0.066)	0.310 (0.067)	0.316 (0.066)	0.310 (0.067)	0.316 (0.066)	0.310 (0.067)
MTF at 10 cyc/deg	0.289 (0.102)	0.299 (0.101)	0.294 (0.101)	0.295 (0.101)	0.299 (0.101)	0.289 (0.102)	0.299 (0.101)	0.289 (0.102)	0.299 (0.101)	0.289 (0.102)
Strehl ratio	0.067 (0.035)	0.070 (0.035)	0.068 (0.034)	0.069 (0.036)	0.070 (0.035)	0.067 (0.035)	0.070 (0.035)	0.067 (0.035)	0.070 (0.035)	0.067 (0.035)

Group ++ corresponds to patients with optical parameter value higher or equal to the median. Group – corresponds to patients with the optical parameter value below the median. The values were accessed by using iTrace, which combines an aberrometer with corneal topography for each eye; a mean was calculated for each participant: mean (SD).

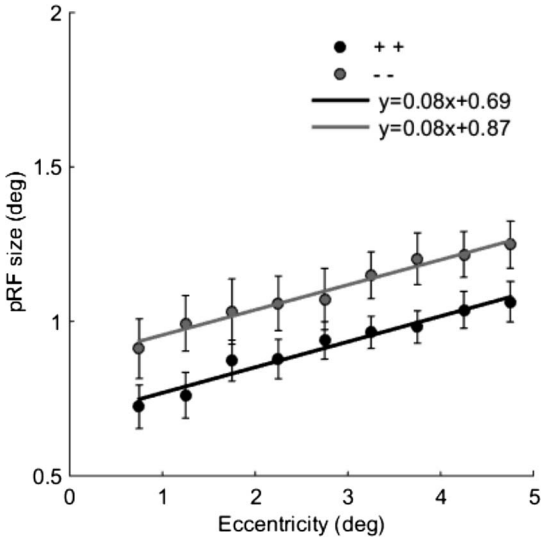

FIGURE 4. Regression analysis of pRF sizes across visual field eccentricity between IOL subgroups defined by MTF_h. The *black* and *gray* colors represent the group of subjects with MTF_h values above (or equal) and below the median, respectively. *Error bars* show the standard error of the mean (SEM) within each eccentricity bin and the *solid lines* show the best significant fit to bin means (P value $<$ 0.0001 for both groups).

obtained in a related study (Rosa AM, et al. *IOVS* 2016;57:ARVO E-Abstract 3756). It is noteworthy that these values were acquired with spectacle correction, whereas the IOL group values were acquired without correction, as the IOL corrects the refractive error almost completely. There is, however, some residual sphere and cylinder in the patient group, which renders some comparisons inadequate. We can, however, compare the RMS-h in both groups, as this is the value of aberrations not correctable with glasses. We observed that they were similar in the patient group and control group (0.16), meaning that IOLs do not introduce significantly different higher-order aberrations across participants relative to the eye's natural optics.

Relation Between Subjective Quality of Vision and pRFs

We evaluated the relation between subjective quality of vision and pRF measures (mean pRF size, β_0, and β_1). Using the total QoV questionnaire score and the "bothersome" (complaint) scores, we divided subjects into two subgroups (low and high score of complaints) on the basis of median value. We compared pRF measures between these subgroups. Surprisingly, subjects with lower total scores (less complaints) had larger pRF sizes across visual field eccentricities (Fig. 5A). These differences between subgroups were mainly explained after taking into account the "bothersome" subscale (Fig. 5B). Importantly, β_0 and β_1 were significantly different between subgroups ($P = 0.012$ and $P = 0.020$, respectively).

Discussion

Our study demonstrated, for the first time, that optical properties of the eye influence pRF sizes and, consequently, cortical resolution of subjects who had undergone recently bilateral sequential cataract surgery, thereby validating the pRF technique in this context. Furthermore, our results showed a striking dissociation between optical parameters/pRFs and the perceived quality of vision, often even in opposing directions.

Through the application of novel stimuli for pRF modelling, we obtained efficient visual field maps similar to those achieved with more conventional stimuli.[10,32] Our pRF modelling results corroborate the commonly described pRF size pattern: pRF size increases as a function of eccentricity.[10,14,47]

There is a gap in the literature in trying to link quantifiable optical outcomes and quality of vision.[48] Our results suggest that studying properties of the visual cortex may be the first step to establish this association. Although it is generally accepted that the brain adapts to adverse/changed visual inputs, the mechanism behind this remains unknown.[49,50] Here, we took a step forward by evaluating the influence of optical parameters (total RMS, RMS of HOAs, modulation transfer function at 10 cyc/deg, and Sthrel ratio) on cortical resolution of patients with recently implanted multifocal IOLs.

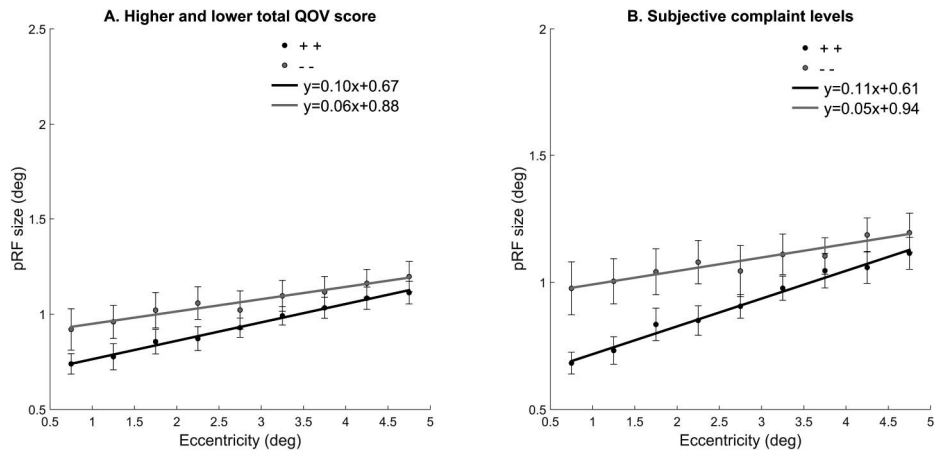

FIGURE 5. Regression analysis of subjective quality of vision and pRF sizes across primary visual cortex. (**A**) Comparison between subjects with higher and lower total quality of vision questionnaire score. (**B**) Comparison between the subjects feeling more or less bothered by dysphotic symptoms. Groups were defined on the basis of the total score and "bothersome" results. The *black* color represents the group with bothersome scoring higher or equal to the median (++) and *gray* color represents the group with bothersome score lower than median (–). *Error bars* show the standard error of the mean (SEM) within each eccentricity bin, and the *solid lines* show the best significant fit to bin means (P value $<$ 0.0001 for both groups). Significant differences were found (**B**) between the intercepts of the linear regression (P value = 0.012) and between the slope of the linear regression ($P = 0.020$).

The study of optical parameters is more relevant shortly after surgery because it is at this time point that we aim to explain objective and subjective visual outcomes in relation to pRFs. In addition, to study the influence of optical properties on pRF sizes, it is necessary to separate this influence from adaptive changes that occur over longer time spans, as it is known that subjects adapt to the blur of their own optical systems.[27] Studying recently operated patients allows assessment of the influence of optical properties on pRF sizes without bias from long-term functional plasticity, which has been shown to occur following cataract surgery (Rosa AM, et al. *IOVS* 2016;57:ARVO E-Abstract 3756). To study the relation between optics and pRFs, the IOL group was divided into two, based on the median value of the aforementioned optical properties. Our results showed that the subgroup with worse optical properties had larger pRF sizes in the striate cortex, as expected. Among all the optical properties that we studied, modulation transfer function seems to influence the most cortical processing. The subgroup of patients with lower values of average MTF_h showed significantly higher mean pRF sizes in the primary visual cortex. The modulation transfer function translates the capacity of the visual system to perceive the contrast of an image at a given spatial resolution and ranges from 0 to 1. In a perfect optical system, modulation transfer function is equal to 1, which indicates that maximum contrast was perceived. Therefore, we demonstrated that patients with lower image contrast also have a coarser cortical resolution. A lower modulation transfer function reflects a loss of perceived image contrast. It can lead to blurring of the retinal image and consequently, larger pRF sizes, as we showed. The pRF size is, in a sense, a byproduct of the eye optics, which shows that retinotopy is able to grasp fine differences in optical properties. Accordingly, as expected, worse optics implies larger pRFs. A striking demonstration of our study was that subjective complaints are dissociable. In other words, changes in pRF sizes reflect measured eye optics, but subjective complaints may often deviate from both.

Therefore, the pRF-based technique is promising for evaluating the influence of optical properties on the measured pRF sizes and can be used to measure changes over time, which will always have to be considered in the context of each patient's optical system.

Our visual perception is not determined merely by the analysis of an optically perfect image, but also by how the brain processes retinal input, as vision involves "constructive" perception. Therefore, we evaluated subjective quality of vision through the validated QoV questionnaire.[29] Surprisingly, patients with more complaints, that is, who felt more bothered by dysphotic symptoms at the third week after cataract surgery, had significantly lower pRF size fitting interceptions and pRF size fitting slopes. This surprising observation shows subjective judgements are more complex than simply predicted from optics and/or cortical parameters.[46] In fact, some patients feel "unhappy" despite having excellent visual acuity measures after cataract surgery.[51] Approximately 0.3% to 12% of these patients require IOL exchange, and even with the new diffractive trifocal intraocular lenses, the number of patients with severe symptoms remains high (approximately 6%).[52–56] It is well known that dysphotic phenomena such as glare, halos, and starbursts (positive dysphotopsia) or even shadows and penumbra (negative dysphotopsia) are one of the main causes for patients' dissatisfaction.[52,53,57] Our results suggest that a more fine-tuned visual processing (with smaller pRF sizes) may allow more intense perception of dysphotic phenomena and therefore paradoxically, worsened subjectively perceived quality of vision. Because these symptoms improve over time in some patients,[52,58] we hypothesize that there are other mechanisms involved in this adaptive process, possibly at a neuronal level, involving higher-level brain regions. A longitudinal cohort study would allow evaluating whether there are alterations at the cortical-processing level after cataract surgery in the long term.

In conclusion, this study highlights the potential use of pRF sizes as a quantitative measure of functional resolution of the visual cortex to objectively assess quality of vision. It shows the tight connection between optical properties and cortical resolution in patients with a recent change in their visual input, in the absence of fully established long-term neuroadaptation, and helps to explain the often observed dissociation between optical parameters and subjectively perceived quality of vision.

Acknowledgments

Supported in part by the Portuguese Funding Agency for Science, Research and Technology (Compete UID/NEU/04539/2013, POCI-01-0145-FEDER-007440); D. Manuel de Mello grant 2014 (José de Mello Saúde, Portugal); Research Support Office grant of the Faculty of Medicine of Coimbra University, Portugal; Clinical Research Awards 2015 of the European Society of Cataract and Refractive Surgeons (ESCRS), BIGDATIMAGE – From computational modelling and clinical research to the development of neuroimaging big data platforms for discovery of novel biomarker, CENTRO-01-0145-FEDER-000016 and ICNAS-Produção.

Disclosure: **Â.S.C. Miranda**, None; **A.F. Martins Rosa**, None; **M.J. Patrício Dias**, None; **B.M. Harvey**, None; **M.F. Loureiro da Silva**, None; **M.S. Castelo-Branco**, None; **J.C.N. Murta**, None

References

1. Kwong KK, Belliveaut JW, Cheslert DA, et al. Dynamic magnetic resonance imaging of human brain activity during primary sensory stimulation. *Proc Natl Acad Sci U S A*. 1992; 89:5675–5679.
2. Bandettini PA, Wong EC, Hinks RS, Tikofsky RS, Hyde JS. Time course EPI of human brain function during task activation. *Magn Reson Med*. 1992;25:390–397.
3. Ogawa S, Tank DW, Menon R, et al. Intrinsic signal changes accompanying sensory stimulation: functional brain mapping with magnetic resonance imaging. *Proc Natl Acad Sci U S A*. 1992;89:5951–5955.
4. Engel SA, Rumelhart DE, Wandell BA, et al. fMRI of human visual cortex. *Nature*. 1994;369:525.
5. Baseler HA, Brewer AA, Sharpe LT, Morland AB, Jägle H, Wandell BA. Reorganization of human cortical maps caused by inherited photoreceptor abnormalities: reorganization of human cortical maps caused by inherited photoreceptor abnormalities. *Nat Neurosci*. 202;5:364–370.
6. Barnes GR, Hess RF, Dumoulin SO, Achtman RL, Pike GB. The cortical deficit in humans with strabismic amblyopia. *J Physiol*. 2001;533:281–297.
7. Victor JD, Apkarian P, Hirsch J, et al. Visual function and brain organization in non-decussating retinal—fugal fibre syndrome. *Cereb Cortex*. 2000;10:2–22.
8. D'Almeida OC, Mateus C, Reis A, Grazina MM, Castelo-branco M. NeuroImage Long term cortical plasticity in visual retinotopic areas in humans with silent retinal ganglion cell loss. *Neuroimage*. 2013;81:222–230.
9. Baker CI, Peli E, Knouf N, Kanwisher NG. Reorganization of visual processing in macular degeneration. *J Neurosci*. 2005; 25:614–618.
10. Dumoulin SO, Wandell BA. Population receptive field estimates in human visual cortex. *Neuroimage*. 2008;39: 647–660.
11. Wandell BA, Dumoulin SO, Brewer AA. Visual field maps in human cortex. *Neuron*. 2007;56:366–383.

12. Victor JD, Purpura K, Katz E, Mao B. Population encoding of spatial frequency, orientation, and color in macaque V1. *J Neurophysiol*. 1994;72:2154–2166.
13. Song C, Samuel D, Kanai R, Rees G. Neural population tuning links visual cortical anatomy to human visual perception. *Neuron*. 2015;85:641–656.
14. Harvey BM, Dumoulin SO. The relationship between cortical magnification factor and population receptive field size in human visual cortex: constancies in cortical architecture. *J Neurosci*. 2011;31:13604–13612.
15. Rodieck RW. Retinal organization. In: *The First Steps in Seeing*. 1st ed. Sunderland, MA: Sinauer Associates; 1998:194–208.
16. Smith AT, Singh KD, Williams AL, Greenlee MW. Estimating receptive field size from fMRI data in human striate and extrastriate visual cortex. *Cereb Cortex*. 2001;11:1182–1190.
17. Wandell BA, Winawer J. Computational neuroimaging and population receptive fields. *Trends Cogn Sci*. 2015;19:349–357.
18. Papanikolaou A, Keliris GA, Lee S, Logothetis NK, Smirnakis SM. NeuroImage nonlinear population receptive field changes in human area V5 / MT + of healthy subjects with simulated visual field scotomas. *Neuroimage*. 2015;120:176–190.
19. Schwarzkopf DS, Anderson EJ, Haas B De, White SJ, Rees G. Larger extrastriate population receptive fields in autism spectrum disorders. *J Neurosci*. 2014;34:2713–2724.
20. Brewer AA, Barton B. Effects of healthy aging on human primary visual cortex. *Health (Irvine Calif)*. 2012;4:695–702.
21. Levin N, Dumoulin SO, Winawer J, Dougherty RF, Wandell BA. Cortical maps and white matter tracts following long period of visual deprivation and retinal image restoration. *Neuron*. 2010;65:21–31.
22. Hoffmann MB, Kaule FR, Levin N, et al. Plasticity and stability of the visual system in human achiasma. *Neuron*. 2012;75:393–401.
23. Duncan RO, Boynton GM. Cortical magnification within human primary visual cortex correlates with acuity thresholds. *Neuron*. 2003;38:659–671.
24. Sabesan R, Yoon G. Visual performance after correcting higher order aberrations in keratoconic eyes. *J Vis*. 2009;9(5):6.
25. Delahunt PB, Webster MA, Ma L, Werner JS. Long-term renormalization of chromatic mechanisms following cataract surgery. *Vis Neurosci*. 2004;21:301–307.
26. Campbell BYFW, Green DG. Optical and retinal factors affecting visual resolution. *J Physiol*. 1965;181:576–593.
27. Artal P, Chen L, Fernández EJ, Singer B, Manzanera S, Williams DR. Neural compensation for the eye's optical aberrations. *J Vis*. 2005;4(4):4.
28. Rosa AM, ÂC, Miranda Patrício M, et al. Functional magnetic resonance imaging to assess the neurobehavioral impact of dysphotopsia with multifocal intraocular lenses. *Ophthalmology*. 2017;124:1280–1289.
29. McAlinden C, Pesudovs K, Moore JE. The development of an instrument to measure quality of vision: The Quality of Vision (QoV) Questionnaire. *Invest Ophthalmol Vis Sci*. 2010;51:5537–5545.
30. McAlinden C, Skiadaresi E, Moore J, Pesudovs K. Subscale assessment of the NEI-RQL-42 Questionnaire with Rasch Analysis. *Invest Ophthalmol Vis Sci*. 2011;52:5685–5694.
31. Brainard DH. The psychophysics toolbox. *Spat Vis*. 1997;10:433–436.
32. Alvarez I, de Haas B, Clark CA, Rees G, Schwarzkopf DS. Comparing different stimulus configurations for population receptive field mapping in human fMRI. *Front Hum Neurosci*. 2015;9:1–16.
33. Zuiderbaan W, Harvey BM, Dumoulin SO. Modeling center-surround configurations in population receptive fields using fMRI. *J Vis*. 2012;12(3):10.
34. Schira MM, Tyler CW, Breakspear M, Spehar B. The foveal confluence in human visual cortex. *J Neurosci*. 2009;29:9050–9058.
35. Dale AM, Fischl B, Sereno MI. Cortical surface-based analysis, I: segmentation and surface reconstruction. *Neuroimage*. 1999;9:179–194.
36. Parker DL, Gullberg GT. Signal to noise efficiency in magnetic resonance imaging. *Med Phys*. 1990;17:250–257.
37. Talairach J, Tournoux P. *Co-Planar Stereotaxic Atlas of the Human Brain. 3-Dimensional Proportional System: An Approach to Cerebral Imaging*. New York: Thieme; 1988.
38. Kriegeskorte N, Goebel R. An efficient algorithm for topologically correct segmentation of the cortical sheet in anatomical MR volumes. *Neuroimage*. 2001;14:329–346.
39. Fischl B, Sereno MI, Dale AM. Cortical surface-based analysis, II: inflation, flattening, and a surface-based coordinate system. 1999;9:195–207.
40. Wandell BA, Chial S, Backus BT. Visualization and measurement of the cortical surface. *J Cogn Neurosci*. 2000;12:739–572.
41. Senden M, Reithler J, Gijsen S, Goebel R. Evaluating population receptive field estimation frameworks in terms of robustness and reproducibility. *PLoS One*. 2014;9:1–30.
42. Sereno M, Dale A, Reppas J, et al. Borders of multiple visual areas in humans revealed by functional magnetic resonance imaging. *Science*. 1995;268:889–893.
43. Larsson J, Heeger DJ. NIH Public Access. *Off J Soc Neurosci*. 2006;26:13128–13142.
44. Dougherty RF, Koch VM, Brewer AA, Modersitzki J, Wandell BA. Visual field representations and locations of visual areas V1/2/3 in human visual cortex. *J Vis*. 2003;3(10):1.
45. Larson AM, Loschky LC. The contributions of central versus peripheral vision to scene gist recognition. *J Vis*. 2009;9(10):6.
46. McAlinden C, Skiadaresi E, Gatinel D, Cabot F, Huang J, Pesudovs K. The Quality of Vision questionnaire: subscale interchangeability. *Optom Vis Sci*. 2013;90:760–764.
47. Amano K, Wandell BA, Dumoulin SO. Visual field maps, population receptive field sizes, and visual field coverage in the human MT+ complex. *J Neurophysiol*. 2009;102:2704–2718.
48. Wilkins MR, Allan BD, Rubin GS, et al. Randomized trial of multifocal intraocular lenses versus monovision after bilateral cataract surgery. *Ophthalmology*. 2013;1290:2449–2456.
49. Rosa AM, Silva MF, Ferreira S, Murta J, Castelo-branco M. Plasticity in the human visual cortex: an ophthalmology-based perspective. 2013;2013:1–13.
50. Pepin S. Neuroadaptation of presbyopia-correcting intraocular lenses. *Curr Opin Ophthalmol*. 2008;19:10–12.
51. Kinard K, Jarstad A, Olson RJ. Correlation of visual quality with satisfaction and function in a normal cohort of pseudophakic patients. *J Cataract Refract Surg*. 2013;39:590–597.
52. de Vries NE, Webers CAB, Touwslager WRH, et al. Dissatisfaction after implantation of multifocal intraocular lenses. *J Cataract Refract Surg*. 2011;37:859–865.
53. Woodward MA, Randleman JB, Stulting RD. Dissatisfaction after multifocal intraocular lens implantation. *J Cataract Refract Surg*. 2009;35:992–997.
54. de Silva SR, Evans JR, Kirthi V, Ziaei M, Leyland M. Multifocal versus monofocal intraocular lenses after cataract extraction (review): multifocal versus monofocal intraocular lenses after cataract extraction. *Cochrane Database Syst Rev*. 2012;(9):3–5.

Investigative Ophthalmology & Visual Science

55. Dick HB, Dell S, Rosen E, Ali JL, Slade S. Efficacy and safety of multifocal intraocular lenses following cataract and refractive lens exchange: metaanalysis of peer-reviewed publications. *J Cataract Refract Surg*. 2016;42:310–328.
56. Mendicute J, Kapp A, Pierre L, et al. Evaluation of visual outcomes and patient satisfaction after implantation of a diffractive trifocal intraocular lens. *J Cataract Refract Surg*. 2016;42:203–210.
57. Holladay JT, Zhao H, Reisin CR. Negative dysphotopsia: the enigmatic penumbra. *J Cataract Refract Surg*. 2012;38:1251–1265.
58. Palomino Bautista C, Carmona González D, Castillo Gómes A, Bescos JA. Evolution of visual performance in 250 eyes implanted with the Tecnis ZM900 multifocal IOL. *Eur J Ophthalmol*. 2009;19:762–768.

Investigative Ophthalmology & Visual Science